Microporous and Mesoporous Materials 261 (2018) 144–149

Contents lists available at ScienceDirect

Microporous and Mesoporous Materials

journal homepage: www.elsevier.com/locate/micromeso

Biomimetic hierarchical walnut kernel-like and erythrocyte-like mesoporous silica nanomaterials: Controllable synthesis and versatile applications

Nanjing Hao, Yuan Nie, John X.J. Zhang*

Thayer School of Engineering, Dartmouth College, 14 Engineering Drive, Hanover, NH 03755, United States

ARTICLE INFO

Keywords:
Hierarchical
Mesoporous silica
Multi-shell
Multi-stack
Shape

ABSTRACT

We developed a facile and controllable strategy to fabricate biomimetic walnut kernel-like mesoporous silica nanomaterial (WMSN) and erythrocyte-like mesoporous silica nanomaterial (EMSN). The former possesses unique multi-shell hollow structure and surface wrinkles while the latter has special multi-stack structure and bowl-shaped depression. These hierarchical materials with distinct structures can be finely tuned by changing the molar ratios of two surfactants, cetyltrimethylammonium bromide and 11-mercaptoundecanoic acid. The mechanism of structural formation through intermolecular interactions was revealed and validated experimentally. The promising potential applications of WMSN and EMSN in adsorption, cellular imaging, drug delivery, and cancer theranostics were further identified.

1. Introduction

Mesoporous silica nanomaterial (MSN) has attracted considerable attentions due to its unique physicochemical properties, such as tunable size and shape, facile surface functionalization, high pore volume, large surface area, and rich porous texture, which endow them with superior availability in separation, adsorption, catalysis, sensing, and biomedicine [1–4]. To meet the increasing needs of emerging applications, much effort has been devoted to the rational design of MSN, especially particle size, pore, and surface parameters [5]. Comparatively, particle shape as another key parameter of MSN has drawn relatively little attention.

Recent studies from both experimental and theoretical perspectives revealed that the shapes of nanoparticles could generate significant impact on their performance [6–8]. Many protocols were developed to produce MSN of different shapes. These included sphere, rod, cube, ellipsoid, film, and sheet [8–10]. However, almost all of these shapes only perform relatively simple dimensions and/or single porous arrangement, and most importantly, these protocols are generally not controllable and tunable for the synthesis of MSN with distinct shapes. Actually, hierarchical materials with multi-level structures could provide abundant pore openings and multistage pore structure, which will be greatly favorable for those involving mass transfer process between the particulate and molecule or organism [11,12]. Therefore, developing a facile protocol for realizing controllable and tunable synthesis of hierarchical MSN with distinct structures is still a major challenge and in great demand.

Herein, we first introduce a facile and controllable protocol to synthesize hierarchical walnut kernel-like mesoporous silica nanomaterial (WMSN) with multi-shell hollow structure and hierarchical erythrocyte-like mesoporous silica nanomaterial (EMSN) with multi-stack structure using cetyltrimethylammonium bromide (CTAB) and 11-mercaptoundecanoic acid (MUA) as co-surfactants. These unique hierarchical materials with distinct structures can be easily tuned by changing the molar ratios of CTAB to MUA. Their formation mechanisms were then revealed and validated experimentally. The potential versatile applications of these hierarchical structures in adsorption, imaging, drug delivery, and cancer theranostics were further examined.

2. Experimental details

2.1. Materials and reagents

Cetyltrimethylammonium bromide (CTAB), 11-mercaptoundecanoic acid (MUA), tetraethyl orthosilicate (TEOS), ammonia (28–30%), rhodamine B (RB), methylene blue (MB), doxorubicin hydrochloride (Dox), fluorescein isothiocyanate (FITC), dimethylformamide (DMF), acetone, 3-Aminopropyltrimethoxysilane (APTMS), Cell-counting kit-8 (CCK-8), and ethanol (200-proof) were purchased from Sigma-Aldrich. Water used was from a Milli-Q water ultrapure water purification system. All chemicals were used as received without any further purification.

* Corresponding author.
E-mail address: john.zhang@dartmouth.edu (J.X.J. Zhang).

https://doi.org/10.1016/j.micromeso.2017.11.003
Received 28 July 2017; Received in revised form 16 September 2017; Accepted 1 November 2017
Available online 05 November 2017
1387-1811/

2.2. Synthesis of hierarchical mesoporous silica materials

Synthesis of WMSN: Briefly, CTAB (0.55 mmol) and MUA (0.46 mmol) were firstly dissolved in the mixed solvents of water (120 mL) and ethanol (40 mL). TEOS (2 mL) and ammonia (~30 mmol) were then separately added with gentle stirring for 3 h at room temperature.

Synthesis of EMSN: Same protocol as above, except for increasing the amount of CTAB from 0.55 mmol to 1.10 mmol.

After collected by centrifugation and followed by washed three times with ethanol, the resulting solid products were dried at 80 °C overnight. Surfactant templates were then removed by gradient calcination (100–600 °C) for 6 h. The resulting solid products were collected for further analysis.

2.3. Rhodamine B and methylene blue adsorption

The adsorption performance of the WMSN and EMSN was evaluated by the adsorptive separation of RB and MB mixture in aqueous solution. All the adsorption experiments were conducted under stirring conditions throughout the test at room temperature in the dark. Typically, the adsorbent (WMSN or EMSN, 5 mg) was added to RB and MB mixed solution (100 mL) with an initial concentration of 10^{-5} mol L^{-1}. At appropriate time intervals (0, 2.5, 5, 10, 15, 30, 60, 120, and 180 min), the aliquots (5 mL) were withdrawn from the suspension and the adsorbents were separated from the suspension via centrifugation. The concentration of the residual RB and MB in the supernatant solution was detected using a UV-visible spectrophotometer. The adsorption rates (C/C_0) were determined at a wavelength of 554 nm and 664 nm for RB and MB, respectively. RB and MB adsorption results were obtained in triplicates.

2.4. Fluorescent labelling of WMSN and EMSN

To track the intracellular behaviour of WMSN and EMSN, FITC molecules were used to conjugate onto particle surface. Briefly, nanoparticles (20 mg) were firstly mixed with APTMS (10 μL) in DMF for grafting amine groups on particle surfaces. Then, FITC (2 mg) was added to a dispersion of the resultant materials in Tris-Cl buffer. The reaction was then allowed to proceed for 36 h at room temperature in the dark. The mixture was centrifuged and the solid was washed thoroughly to remove non-conjugated FITC. The final products, WMSN-FITC and EMSN-FITC, were dispersed in PBS (pH 7.2) and stored in a dark place.

2.5. Loading and releasing of doxorubicin (Dox)

To load Dox into WMSN and EMSN, nanomaterials were firstly dispersed in an aqueous solution of Dox (25 mg mL^{-1}) while keeping the weight ratio of nanoparticles to drug at 1:1. The mixture was stirred at 37 °C for 36 h under dark conditions, followed by centrifugation and washing twice with water to obtain the drug-loaded hierarchical nanomaterials (WMSN-Dox and EMSN-Dox). The loading amount of Dox was determined by UV/vis spectroscopy at 233 nm using a standard calibration curve of Dox. For cellular imaging test, WMSN-FITC and EMSN-FITC were treated in the same protocol as above.

For the drug release, WMSN-Dox and EMSN-Dox samples were immersed in PBS (pH 4.5 and pH 7.2), and the supernatant was collected at given time intervals (0, 1, 2, 4, 8, 12, 16, 24, 36, and 48 h). The absorbance at 233 nm was measured to determine the amount of Dox released. Drug releasing results were obtained in triplicates.

2.6. Cellular uptake and cell imaging analysis

SK-BR-3 cells (human breast cancer cell line, ATCC) were maintained in high glucose DMEM (Dulbecco's Modified Eagle's Medium, ATCC) supplemented with 10% FBS (ATCC) and 1% penicillin-streptomycin (Sigma) in a humidified incubator at 37 °C with 5% CO_2 and 95% air. For intracellular localization, 10^5 SK-BR-3 cells per well were seeded in a 6-well plate containing cover glasses and were allowed to adhere for 24 h. After incubation with 50 μg mL^{-1} Dox-loaded FITC-labeled WMSN and EMSN for 3 h, the cover glass containing SK-BR-3 cells were washed with PBS and was then mounted onto a glass slide. The slide was examined under a fluorescence microscope (Olympus BX51).

2.7. In vitro cytotoxicity evaluation

The cytotoxicity of WMSN, EMSN, WMSN-Dox, EMSN-Dox, and free Dox was evaluated using the CCK-8 viability assay. For the cytotoxicity evaluation, SK-BR-3 cells were seeded at a density of 8000 cells per well in 96-well plates. After incubating the SK-BR-3 cells with WMSN, EMSN, WMSN-Dox, EMSN-Dox, and free Dox for 24 h, 10 μL CCK-8 reagent was added to each well and incubated for 4 h. The absorbance of the resulting solution in each well was recorded at 450 nm with a microplate reader (TECAN SPARK 10M). Before reading, the plate was gently shaken on an orbital shaker for 30 s to ensure homogeneous distribution of color.

3. Results and discussion

Hierarchical mesoporous silica nanoparticles having multi-level structures can be successfully fabricated using CTAB and MUA as co-surfactants, tetraethyl orthosilicate (TEOS) as silica precursor, and ammonia as catalyst in the mixed solvents of water and ethanol. As shown from the SEM images in Fig. 1, WMSN and EMSN perform typical walnut kernel-like structure with rich surface wrinkles (Fig. 1A–C) and erythrocyte-like structure with flat and bowl-shaped depression (Fig. 1G–I), respectively. From the TEM images, it is interesting to find that WMSN has unique hollow and multi-shell structure (Fig. 1D–F), while EMSN has special sandwich-like and multi-stack structure (Fig. 1J–L). In addition, WMSN has an average size of ~300 nm, and EMSN has an average size of ~200 nm and an average thickness of ~50 nm. The porous properties of WMSN and EMSN were further determined by nitrogen adsorption-desorption analysis after removing the surfactants by calcination (Fig. S1). The results showed that both materials exhibited typical type IV isotherm with H3 hysteresis (Figs. S2A and S3A) [13,14], and multiple pore size distributions can be observed (Figs. S2B and S3B), indicating the presence of hierarchical porous structures. This finding is in good agreement with the above SEM and TEM investigations. The Brunauer-Emmett-Teller (BET) surface area and pore volume of WMSN were measured to be 579.6 m^2/g and 0.44 cm^3/g, respectively. Whereas, the BET surface area and pore volume of EMSN were slightly increased to 733.5 m^2/g and 0.58 cm^3/g, respectively. Both materials have similar Barrett-Joyner-Halenda (BJH) pore size at around 3.0 nm.

To explore the formation mechanism of these unique hierarchical materials with distinct structures, a series of experiments were carried out to examine the role of each reaction reagent (CTAB, MUA, TEOS, ammonia, water, and ethanol) and how it works for building these hierarchical architectures. It was found that only CTAB and MUA (i.e., molar ratios of CTAB to MUA) exhibit major implications in particle shape regulation while others (TEOS, ammonia, water, and ethanol) play relatively minor functions. As shown in Fig. 2, at different R values (R = molar ratio of CTAB to MUA), the resultant products perform different shapes. At R = 0.5, hierarchical material with abundant irregular surface wrinkles was obtained, but there was no obvious multi-shell structure. When R was increased to 1, mesoporous silica product with typical multi-shell hollow structure was formed. Similar as WMSN, this product also has well-defined hierarchical shape. However, if R was set at 2 and 3, flat products with bowl-shaped depression can be obviously observed. Both kinds of products also possess hierarchical

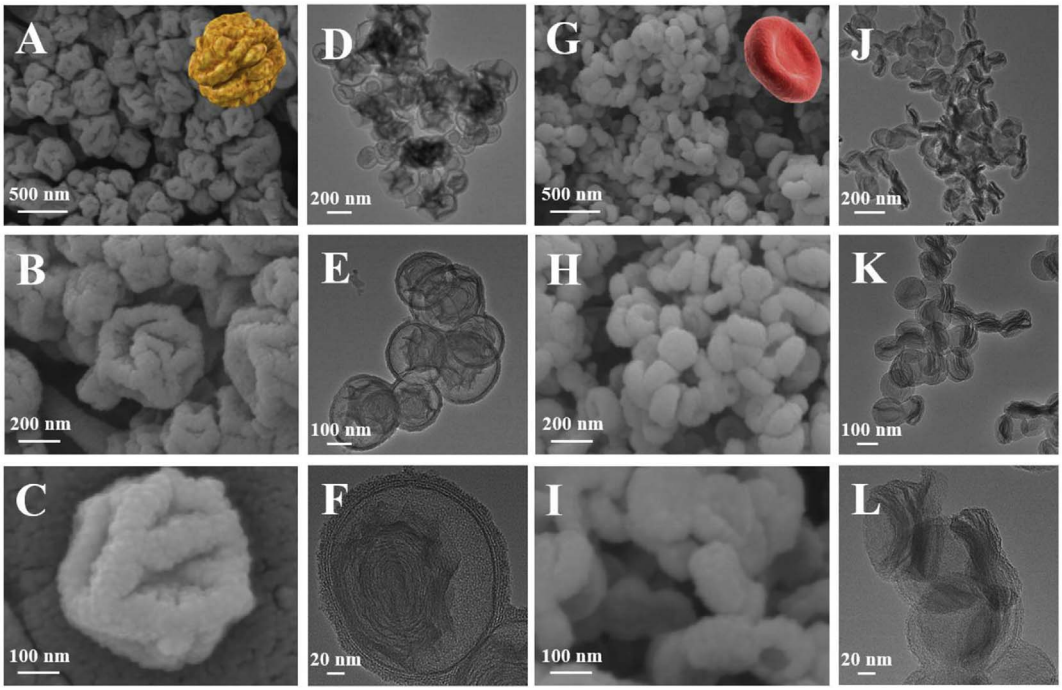

Fig. 1. Scanning electron microscopy (SEM, A-C and G-I) and transmission electron microscopy (TEM, D-F and J-L) images of hierarchical walnut kernel-like mesoporous silica nanomaterial (WMSN, A-F) and erythrocyte-like mesoporous silica nanomaterial (EMSN, G-L). The insets in A and G are the images of walnut kernel and erythrocyte, respectively. The SEM images were acquired after gold sputtering.

structures similar as EMSN, and typical multi-stack shape can be seen clearly especially for the product from R at 3 protocol. In addition, when R was further increased to 5, the final product turned into a near-spherical shape and no hierarchical structure can be obtained. Moreover, there was no obvious product formed using only MUA as surfactant, whereas, typical spherical mesoporous silica nanoparticles can be obtained using only CTAB as surfactant (Fig. S4).

Based on the above observations, we proposed possible mechanisms to explain the formation of such hierarchical structures in the presence of CTAB and MUA surfactants (Fig. 3). Both CTAB and MUA took part in the shape formation process and determined the structural transition from multi-shell to multi-stack. It is generally suggested that the growth of mesoporous silica is initiated by the interactions between the silica precursor and the surface of CTAB vesicles [15]. In this system, MUA plays a significant role in the self-assembly of surfactants and assists in the formation of different hierarchical structures. When the molar ratios of CTAB to MUA are relatively low (R = ~1), CTAB (a cationic surfactant) and MUA (an anionic surfactant) can self-assemble into typical vesicles in basic conditions [16]. After the CTAB/MUA vesicles have formed in the mixed solvents of water and ethanol, TEOS molecules as silica precursor will attach to the surfaces of the vesicles through electrostatic attraction. The regions near the vesicle surfaces will thus gain a higher concentration of TEOS [17,18]. Meanwhile, the vesicle formed from CTAB/MUA may undergo deformations when they divided

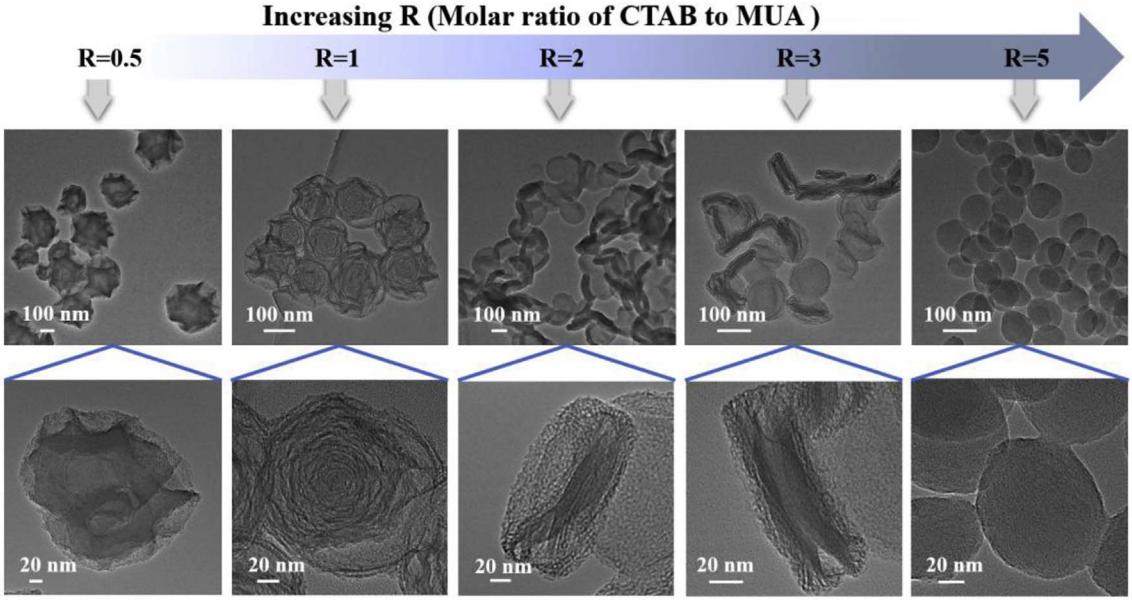

Fig. 2. The effect of the molar ratio of CTAB to MUA on the morphology change of MSN.

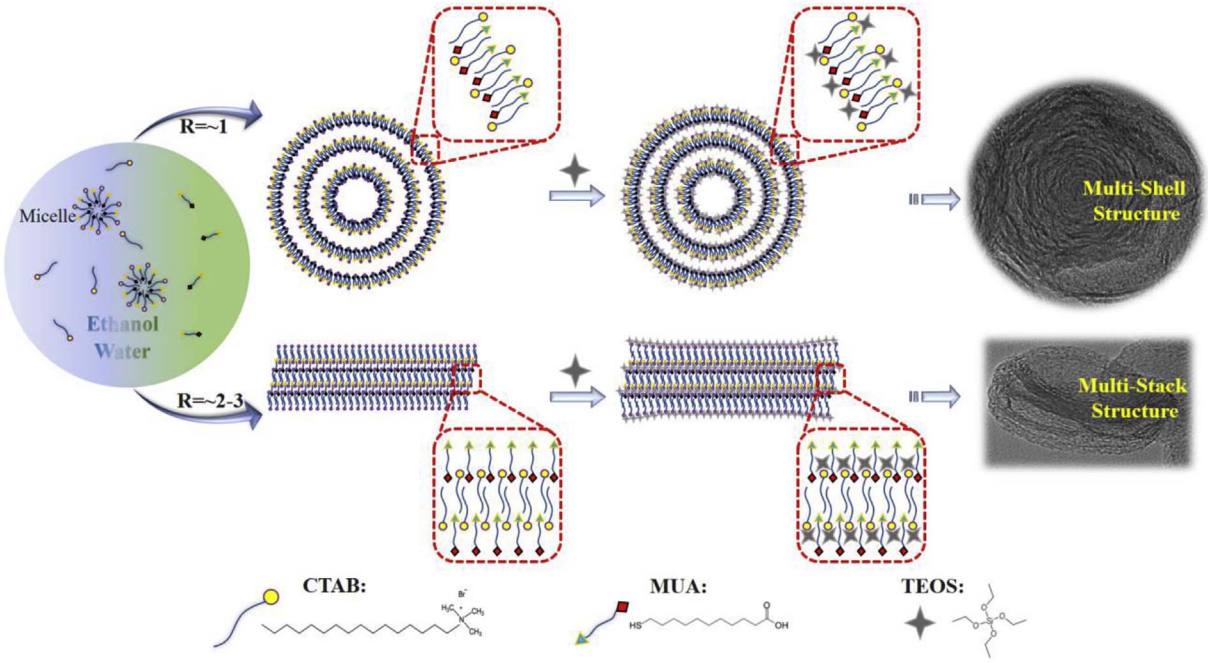

Fig. 3. Mechanism for the Formation of hierarchical mesoporous silica nanoparticles with multi-shell and multi-stack structures.

into smaller but more stable vesicles for forming multi-lamellar vesicles [17–20]. Accompanied by the sustaining hydrolysis and cocondensation of TEOS, these multi-lamellar vesicles will continuously interact with silica species to produce composite vesicles, and further evolve into hierarchical nanoparticles with multi-shell structure (Similar as WMSN) (Fig. 3). Comparatively, if the reaction is performed at higher molar ratios of CTAB to MUA (R = ~2–3), the CTAB-rich multi-lamellar vesicles are generally not easily formed because of the bending energy consideration [17,21]. Therefore, CTAB and MUA surfactants will be alternatively present multi-lamellar stacks structure (Fig. 3). Due to the region-dependent effects [11], in the inside region of multi-lamellar stacks, the relatively higher external surface pressure will lead to bowl-shaped depression, whereas, in the edge region, the diffusion of ethanol into multi-lamellar stacks reduces the interaction of the alkyl tails and thus increases the hydrophobic volume of multi-lamellar stacks [22]. This situation further makes such multi-lamellar stacks generate hierarchical nanoparticles with multi-stack structure (Similar as EMSN) (Fig. 3).

Owing to their unique hierarchical shape, multi-level structure, high pore volume, large surface area, and multiple pore size distributions, both WMSN and EMSN could be greatly favored in many application fields, especially those involving mass transfer process. To demonstrate this, we firstly examined the adsorption capacity of WMSN and EMSN toward Rhodamine B (RB) and Methylene Blue (MB) (Fig. 4A). As shown in Fig. 4B–C, even at a low mass ratio of adsorbent (WMSN or EMSN) to adsorbate (RB and MB mixture) (Table S1) [23–25], the characteristic absorption of RB at 554 nm and MB at 664 nm decreased dramatically in the first 30 min. This phenomenon, except for the presence of electrostatic interactions between the positively charged dyes (RB and MB) and the negatively charged silicate surface, may be probably attributed to the special shape of both hierarchical materials with unique multi-level structures (Table S1). Subsequently, the remaining concentration changes of RB and MB slowed with increasing adsorption time (Fig. 4B–C). This result agreed well with the sample photos that were recorded at the corresponding different time intervals (Figs. S5–6). The removal rate of RB and MB by WMSN or EMSN as a function of time also clearly confirmed that such adsorption process is fast, especially in the early stage. After 30 min, RB and MB can be nearly completely removed accompanying the disappearance of the purple color (Figs. S5–6). In addition, it is noted that both materials exhibit higher and faster adsorption of MB than that of RB due to the relatively smaller molecular size of MB compared to that of RB (Fig. 4A).

To further examine the potential of these hierarchical materials, WMSN and EMSN were labeled with fluorescein isothiocyanate (FITC) and loaded with Doxorubicin (Dox, an anticancer drug) for cellular imaging, drug delivery, cytocompatibility, and cancer cell inhibition performance tests. As shown in Fig. 5A–B, after SK-BR-3 cells were treated with the FITC-labeled Dox-loaded WMSN or EMSN, the green color from FITC and the red color from Dox can be obviously seen from inside of cells, indicating that both WMSN and EMSN can be efficiently internalized into cells and then release Dox there. The loading amounts of Dox were determined to be as high as 367.4 mg per gram of WMSN and 283.3 mg per gram of EMSN, respectively (Table S2), indicating the superior capacity of these hierarchical structures as a drug nanocarrier. The release profiles of Dox from Dox-loaded WMSN (WMSN-Dox) and Dox-loaded EMSN (EMSN-Dox) were then measured in pH 4.5 and pH 7.2 PBS to simulate different physiological conditions. As shown in Fig. 5C, Dox can be gradually released from WMSN-Dox and EMSN-Dox in a pH-dependent way. At pH 7.2, because of electrostatic attraction and hydrogen bonding interactions between Dox and silica matrix, both WMSN-Dox and EMSN-Dox exhibited relatively slow release profile, and only around 15% of Dox was released after 48 h. Comparatively, acidic condition (pH 4.5) allows to decrease the density of the hydrogen bonding and as a result the Dox release is enhanced. The cumulative drug release rates were thus increased to 60.4% and 71.3% for WMSN-Dox and EMSN-Dox, respectively. The release profiles displayed typical sustained and multistage behavior, which is probably attributed to the hierarchical shapes of WMSN and EMSN with multi-level structure [26–28]. Cytocompatibility test using SK-BR-3 cells suggested that there is no significant adverse effect for WMSN and EMSN even at a high particle concentration of 0.5 mg/mL (Fig. 5D). The cancer cell inhibition performance of WMSN-Dox and EMSN-Dox was further investigated and compared with free Dox (Fig. 5E). Results showed that free Dox, WMSN-Dox, and EMSN-Dox all have obvious cell inhibition after 24 h incubation with Dox concentration range from 0.01 to 1 μM. However, the half inhibitory concentration (IC_{50}) of Dox is 2.5-fold of WMSN-Dox and 3.3-fold of EMSN-Dox, respectively. Compared to free

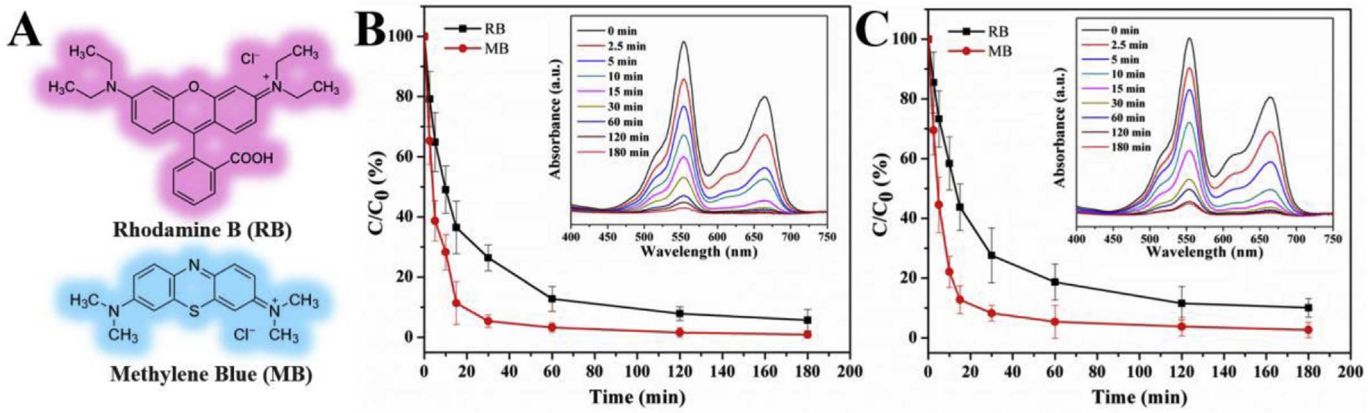

Fig. 4. Adsorption of Rhodamine B (RB) and Methylene Blue (MB). (A) Chemical structures of RB and MB. (B-C) Adsorption rates of the mixture of RB and MB by WMSN (B) and EMSN (C). C_0 is the initial concentration of the RB and MB solution (Both at 10^{-5} M), and C is the concentration of that at different time intervals during the adsorption. Error bars show the standard deviations from three independent tests. The insets in (B) and (C) are a group of UV−vis spectra for time-dependent adsorption of RB and MB in the presence of WMSN and EMSN, respectively.

Dox, the increased cytotoxicity of WMSN-Dox and EMSN-Dox may be probably caused by the enhanced drug nanocarrier uptake by SK-BR-3 cells and the following targeted drug release inside of cells. In addition, the relatively higher cell inhibition rate of EMSN-Dox than that of WMSN-Dox also agrees well with their drug release profiles (Fig. 5C).

4. Conclusions

In summary, we first developed a facile and controllable strategy to synthesize hierarchical WMSN with unique multi-shell hollow structure and rich surface wrinkles and hierarchical EMSN with special multi-stack structure and bowl-shaped depression using CTAB and MUA as co-surfactants. It was found that only CTAB and MUA (i.e., molar ratios of CTAB to MUA) exhibit major implications in particle shape regulation whereas others (TEOS, ammonia, water, and ethanol) play relatively minor roles. Their formation mechanisms were further revealed and validated experimentally. Such hierarchical structures exhibited superior performance in the adsorption of RB and MB, cellular imaging,

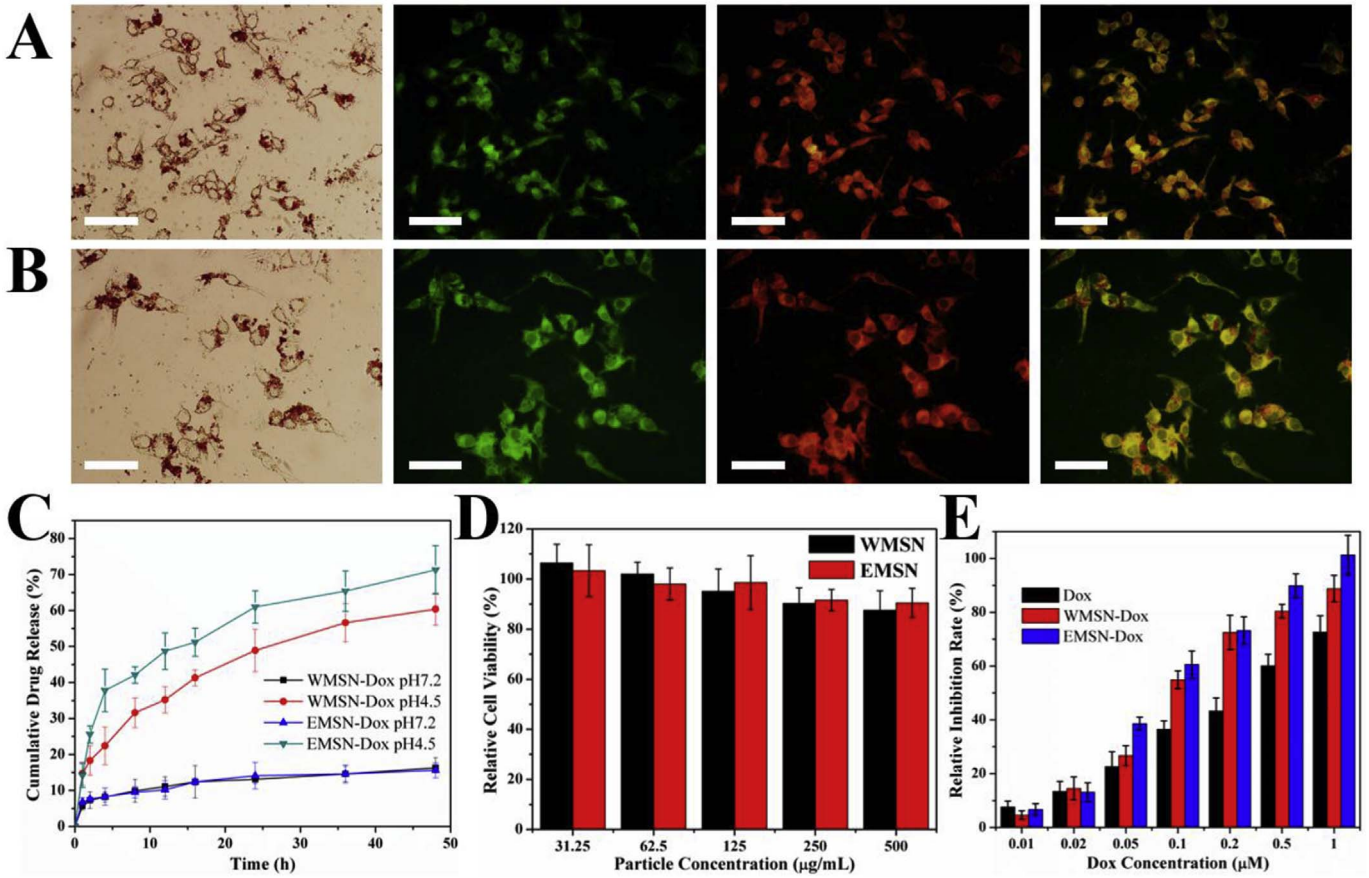

Fig. 5. (A-B) Images of SK-BR-3 cells after treating with Dox-loaded FITC-labeled WMSN (A) or EMSN (B) for 3 h. From left to right: bright-field image, FITC image, doxorubicin image, and merged FITC and doxorubicin image. Scale bars = 50 μm. (C) Release profile of Dox from WMSN-Dox and EMSN-Dox in PBS buffer (pH 4.5 and pH 7.2); (D) SK-BR-3 cell viability with particle concentrations of WMSN and EMSN from 31.25 to 500 μg mL^{-1} for 24 h. (E) Inhibition rates of Dox, WMSN-Dox, and EMSN-Dox (at concentration range of Dox from 0.01 to 1 μM) on SK-BR-3 cells for 24 h.

Dox drug delivery, and cancer cell inhibition. Owing to their biomimetic hierarchical shape, multi-level structure, high pore volume, large surface area, and multiple pore size distributions, these materials hold great potential for the advancement of versatile practical applications.

Acknowledgment

This work was sponsored by the NIH Director's Transformative Research Award (R01HL137157), and NSF grants (ECCS 1128677, 1309686, 1509369). We gratefully acknowledge the support from the Electron Microscope Facility at Dartmouth College.

Appendix A. Supplementary data

Supplementary data related to this article can be found at http://dx.doi.org/10.1016/j.micromeso.2017.11.003.

References

[1] N.J. Hao, K. Neranon, O. Ramström, M. Yan, Biosens. Bioelectron. 76 (2016) 113–130.
[2] A.S. Dias, M. Pillinger, A.A. Valente, Microporous Mesoporous Mater 94 (2006) 214–225.
[3] C. Knöfel, J. Descarpentries, A. Benzaouia, V. Zeleňák, S. Mornet, P.L. Llewellyn, V. Hornebecq, Microporous Mesoporous Mater 99 (2007) 79–85.
[4] Y. Zhu, J. Shi, Y. Li, H. Chen, W. Shen, X. Dong, Microporous Mesoporous Mater 85 (2005) 75–81.
[5] N.J. Hao, L.F. Li, F.Q. Tang, Int. Mater. Rev. 62 (2017) 57–77.
[6] K. Yang, Y.Q. Ma, Nat. Nanotechnol. 5 (2010) 579–583.
[7] Y. Geng, P. Dalhaimer, S.S. Cai, R. Tsai, M. Tewari, T. Minko, D.E. Discher, Nat. Nanotechnol. 2 (2007) 249–255.
[8] N.J. Hao, L. Li, Q. Zhang, X. Huang, X. Meng, Y. Zhang, D. Chen, F. Tang, L. Li, Microporous Mesoporous Mater 162 (2012) 14–23.
[9] N.J. Hao, F.Q. Tang, L.F. Li, Microporous Mesoporous Mater 218 (2015) 223–227.
[10] N.J. Hao, L.F. Li, F.Q. Tang, Biomater. Sci. 4 (2016) 575–591.
[11] N.J. Hao, H.T. Chorsi, J.X.J. Zhang, ACS Sustain. Chem. Eng. 5 (2017) 2044–2049.
[12] N.J. Hao, L.F. Li, F.Q. Tang, J. Nanopart. Res. 18 (2016) 321.
[13] K.S.W. Sing, D.H. Everett, R.A.W. Haul, L. Moscou, R.A. Pierotti, J. Rouquerol, T. Siemieniewska, Pure Appl. Chem. 57 (1985) 603–619.
[14] M. Kruk, M. Jaroniec, Chem. Mater 13 (2001) 3169–3183.
[15] C.T. Kresge, M.E. Leonowicz, W.J. Roth, J.C. Vartuli, J.S. Beck, Nature 359 (1992) 710–712.
[16] X.J. Wu, D.S. Xu, J. Am. Chem. Soc. 131 (2009) 2774–2775.
[17] J. Liu, S.B. Hartono, Y.G. Jin, Z. Li, G.Q. Lu, S.Z. Qiao, J. Mater. Chem. 20 (2010) 4461–4728.
[18] J. Liu, T.Y. Yang, D. wei Wang, G.Q. Lu, D.Y. Zhao, S.Z. Qiao, Nat. Commun. 4 (2013) 2798.
[19] H.L. Xu, W.Z. Wang, Angew. Chem. Int. Ed. 46 (2007) 1489–1492.
[20] J. Qi, X.Y. Lai, J.Y. Wang, H.J. Tang, H. Ren, Y. Yang, Q. Jin, L.J. Zhang, R.B. Yu, G.H. Ma, Z.G. Su, H.J. Zhao, D. Wang, Chem. Soc. Rev. 44 (2015) 6749–6773.
[21] X. Gu, C.L. Li, X.H. Liu, J.W. Ren, Y.Q. Wang, Y.L. Guo, Y. Guo, G.Z. Lu, J. Phys. Chem. C 113 (2009) 6472–6479.
[22] Z.G. Teng, G.F. Zheng, Y.Q. Dou, W. Li, C.Y. Mou, X.H. Zhang, A.M. Asiri, D.Y. Zhao, Angew. Chem. Int. Ed. 51 (2012) 2173–2177.
[23] S. Wang, Z.H. Zhu, J. Hazard. Mater 136 (2006) 946–952.
[24] S. Eftekhari, A. Habibi-Yangjeh, S.H. Sohrabnezhad, J. Hazard. Mater 178 (2010) 349–355.
[25] S. Wang, H.T. Li, L.Y. Xu, J. Colloid Interf. Sci. 295 (2006) 71–78.
[26] N.J. Hao, K.W. Jayawardana, X. Chen, M. Yan, ACS Appl. Mater. Interfaces 7 (2015) 1040–1045.
[27] N.J. Hao, Y. Nie, A. Tadimety, A.B. Closson, X.J. Zhang, Mater. Res. Lett. 8 (2017) 584–590.
[28] Y. Li, B.P. Bastakoti, Y. Yamauchi, Chem. Eur. J. 21 (2015) 8038–8042.